

# A new chronology for the Moon and Mercury

Simone Marchi

*German Aerospace Center (DLR), Institute of Planetary Research, Rutherfordstr. 2, D-12489 Berlin  
Dipartimento di Astronomia, Università di Padova, Vicolo dell'Osservatorio 2, I-35122 Padova*

`simone.marchi@unipd.it`

Stefano Mottola

*German Aerospace Center (DLR), Institute of Planetary Research, Rutherfordstr. 2, D-12489 Berlin*

Gabriele Cremonese

*INAF, Osservatorio Astronomico di Padova, Vicolo dell'Osservatorio 3, I-35122 Padova*

Matteo Massironi

*Dipartimento di Geoscienze, Università di Padova, via Giotto 1, I-35137, Padova*

and

Elena Martellato

*INAF, Osservatorio Astronomico di Padova, Vicolo dell'Osservatorio 3, I-35122 Padova*

## ABSTRACT

In this paper we present a new method for dating the surface of the Moon, obtained by modeling the incoming flux of impactors and converting it into a size distribution of resulting craters. We compare the results from this model with the standard chronology for the Moon showing their similarities and discrepancies. In particular, we find indications of a non-constant impactor flux in the last 500 Myr and also discuss the implications of our findings for the Late Heavy Bombardment hypothesis. We also show the potential of our model for accurate dating of other inner Solar System bodies, by applying it to Mercury.

*Subject headings:* solar system: general — planets and satellites: Earth, Mercury, Moon

## 1. Introduction

Craters are among the most spectacular surface features of the solid bodies of the Solar System. Cratering studies provide a fundamental tool for the age determination of planetary and asteroidal terrains. Since the beginning of the lunar exploration, age estimates for the lunar terrains were derived, followed by chronology models for the other terrestrial planets. The development of the lunar chronology greatly helped in interpreting

the evolution of the Solar System and in particular of our own planet, the Earth. Recently, thanks to a fleet of new space missions (Mars Express to Mars, MESSENGER to Mercury, and Kaguya to the Moon, only to name a few), this field of research entered a new exciting phase, where accurate age estimates provide means for detailed small-scales geological studies.

The method currently used for dating purposes defines a chronology (crater surface density vs. absolute age) for a reference body for which ra-

radiometric ages are available for different terrains. Then, on the basis of models predicting the impactor flux ratio between the reference body and another generic body, it is possible to estimate the age of the latter. This method can be defined *experimental*, since it develops a chronology of a reference body for which two measurable quantities are available: absolute ages and number of craters for selected areas. The Moon is the only body of the Solar System that could fulfill both requirements so far. This method has been developed and refined in the last 30 years by many researchers and represents the reference for dating purposes (e.g. Hartmann et al. 1981; Neukum 1983). In this approach, the development of the chronology for the reference body does not depend explicitly on the physics of the cratering process. However, such information becomes necessary -via a cratering scaling law- in order to apply the Moon chronology to other bodies or to infer the flux of impactors from the observed cratering record.

A possible alternative -purely *theoretical*- approach could be based on the accurate estimation of the time-dependent impactor flux for each target body, through the history of the Solar System. With this method, a direct comparison between the observed distribution of craters on a given terrain and the isochrones produced by the model would give its age. Although the knowledge of the formation and evolution of the Solar System greatly improved in recent years, such ambitious goal is presently far beyond the capabilities of the available models, due to the large uncertainties in the early stages of its formation.

In this paper we introduce a third approach for determining the chronology of objects in the inner Solar System. This method, which can be considered as a *hybrid* of the first two approaches, is based on the dynamical model by Bottke et al. (2000, 2002, 2005a,b) which describes the formation and evolution of asteroids in the inner Solar System. In this framework, first the flux of impactors on the Moon is derived, then the impactor size distribution is converted into a cumulative crater distribution via an appropriate scaling law, and finally the radiometric ages of different regions -the Apollo and Luna landing sites- are used for the calibration of the lunar chronology. The main advantage of our approach is that the adopted model naturally describes the distributions of the

impactor sizes and velocities for any body in the inner Solar System. Thus, the lunar calibration can be exported with precision to any other body. A drawback of the method, however, is that the chronology of the reference body depends -through the scaling law- on the physics of the cratering process, which is as yet not fully understood. Furthermore, the precision of the age estimate relies on the accuracy of the dynamical model. Encouragingly, the adopted dynamical model is capable of providing a good representation of the present asteroid population and size distribution both in the near-Earth space and in the main belt, with a maximum deviation amounting to less than a factor of 2 (Bottke et al. 2005b).

## 2. Modeling the cratering on the Earth-Moon system

The present inner Solar System is continuously reached by a flux of small bodies having sizes smaller than few tens of km. A fraction of these bodies (namely those having perihelion  $< 1.3$  AU) are called near-Earth objects (NEOs). Contributors to this flux are represented by main belt asteroids (MBAs) and Jupiter family comets (JFCs). Both contributions have been modeled by a number of authors and it is generally accepted that the MBAs constitute the main source for the flux presently observed in the inner Solar System (e.g. Morbidelli et al. 2002), therefore we neglect the cometary contribution. This flux is sustained by a few fast escape tracks, which are continuously replenished with new bodies as a result of collisional processes and semimajor axis mobility. The main gateways to the inner Solar System are the  $\nu_6$  secular resonance with Saturn and the 3:1 mean motion resonance with Jupiter (Morbidelli & Gladman 1998; Morbidelli et al. 2002). One of the most recent and accurate models concerning NEOs formation has been developed by Bottke et al. (2000, 2002), while Bottke et al. (2005a,b) modeled the main belt dynamical evolution. These models have been adopted in order to estimate the properties of the impactor flux at the Moon.

## 2.1. Modeling the impactor flux: the stationary case

The flux of impactors may be described as a differential distribution,  $\phi(d, v)$ , which represents the number of incoming bodies per unit of impactor size ( $d$ ) and impact velocity ( $v$ ). An important quantity -since it can be constrained from observations- is the size distribution of the incoming bodies, namely the number of impactors per unit impactor size. Let  $h(d)$  be such distribution, we then have:  $h(d) \equiv \int \phi(d, v) dv$ . Therefore, without loss of generality, we can write:

$$\phi(d, v) = h(d)f(d, v) \quad (1)$$

where  $f(d, v)$  is the distribution of the impact velocities (i.e. the impact probability per unit impact velocity) for any dimension  $d$ , and which fulfills the normalization constraint  $\int f(d, v) dv \equiv 1$ . We used the NEO orbital distribution model computed by Bottke et al. (2000, 2002), generated by integrating two sets of test particles placed into the  $\nu_6$  and 3:1 resonances (with  $2 \times 10^6$  and  $7 \times 10^5$  particles, respectively). For each particle they computed the impact probability and the impact velocity relative to the target body. Following the work of Marchi et al. (2005), we computed the impact velocity distribution (corrected for the gravitational cross-section of the targets). We assumed that the Moon revolves around the Sun with an orbit identical to that of the Earth. Moreover, we corrected the impact probability provided by the Bottke et al model in order to account for the different collisional life-time of the particles. This is necessary because the orbital evolution of the particles is coupled with their size through the relationship  $\tau \propto \sqrt{d}$  (Farinella et al. 1998; Bottke et al. 2005b), with  $\tau$  being the particles' collisional life-time. In figure 1 we show the resulting impactor velocity distribution  $f(d, v)$  for the two extreme size bins used in our simulations and for both the Moon and the Earth<sup>1</sup>.

<sup>1</sup>The overall shape of the distributions vaguely resembles a Maxwellian distribution. It is interesting that the distributions have a large number of high velocity (i.e.  $> 20$  km/s) impactors. This distribution may help to explain some anomalies found for some terrestrial impact craters. In particular, only 3 out of about 60 known craters with ages  $< 60$  Myr have been at present associated to tektite strewn fields (French 1998). Since tektites are highly shocked super-heated melts ejected during hypervelocity impacts

The impactor size distribution for the Earth ( $h_e$ ) can be written as follows:

$$h_e(d) = P_e h_n(d) \quad (2)$$

where  $h_n$  is the NEO differential size distribution and  $P_e$  is the intrinsic collision probability. Following Bottke et al. (2005b), we adopted  $P_e = 2.8 \cdot 10^{-9} \text{ yr}^{-1}$ . The distribution  $h_n$  has been derived from Bottke et al. (2002), and it can be scaled to the Moon and other bodies. In the case of the Moon, this is done considering the Earth-Moon ratio of the impact probability as a function of impactor size (Marchi et al. 2005). Let  $\Sigma(d)$  be this ratio, then the Moon impactor size distribution becomes:

$$h_m(d) = P_e h_n(d) \Sigma(d) \quad (3)$$

In figure 2 the cumulative impactor size distribution for both the Moon and the Earth are shown. A similar approach can also be used for evaluating the flux on other targets, like Mercury (see section 6). In equation 1 the dependence of  $h$  and  $f$  over time is neglected since we are considering a stationary problem, while eq. 2 and 3 strictly describe the present flux. Arguments about possible variations in the flux intensity and shape have been discussed since the late 70s, and this still remains one of the most debated topics in the field of lunar cratering. In their work, Neukum and coworkers (e.g. Neukum 1983; Neukum & Ivanov 1994) generally assume a constant shape of the impactor size distribution over time, while others claim a sudden change in the shape after the Late Heavy Bombardment (LHB), about 3.8 Gyr ago (e.g. Strom et al. 2005). One of the potentials of our model is that we can implement and evaluate the effects of a time-dependent size-distribution on the crater cumulative distribution, as shown in section 5.

## 2.2. The scaling law

In order to convert the flux of impactors into a resulting crater distribution, we need to apply

(e.g. Glass 1990; Koeberl et al. 1996), from simple statistical arguments we may estimate that a threshold perpendicular impact velocity of at least 24 km/s is required for their formation (more than 33 km/s modulus for a  $\pi/4$  impacting angle).

a so-called crater-scaling law. Such scaling law attempts to describe the outcome of a cratering event based on the impact energy and on the physical properties of both the target and the projectile. Once an appropriate scaling law is chosen, we may write the final crater diameter  $D$  as a function of the impactor diameter, impact velocity, and a number of parameters (density, strength... indicated by  $\vec{p}$ ), namely  $D = \mathcal{S}(d, v, \vec{p})$ . Despite the great effort (both computational and experimental) devoted to this task, the physics of crater formation is far from being completely understood. For this reason, we decided to explore how the predicted crater distribution depends on the choice of the scaling law. For this purpose we considered the three scaling laws most used in this field. The first one by Holsapple & Housen (2007) (H&H hereinafter), reads:

$$D = kd \left[ \frac{gd}{2v_{\perp}^2} \left( \frac{\rho}{\delta} \right)^{\frac{2\nu}{\mu}} + \left( \frac{Y}{\rho v_{\perp}^2} \right)^{\frac{2+\mu}{2}} \left( \frac{\rho}{\delta} \right)^{\frac{\nu(2+\mu)}{\mu}} \right]^{-\frac{\mu}{2+\mu}} \quad (4)$$

where  $g$  is the target gravitational acceleration,  $v_{\perp}$  is the perpendicular component of the impactor velocity,  $\delta$  is the projectile density,  $\rho$  and  $Y$  are the density and tensile strength of the target. The quantities  $k$  and  $\mu$  depend on the target material and  $\nu$  on its porosity. H&H estimated these latter parameters by best-fitting over a range of experiments done with different materials. From this study we adopted the values  $k = 1.03$  and  $\mu = 0.41$  for cohesive soils, and  $k = 0.93$ ,  $\mu = 0.55$  for rocks. We used  $\nu = 0.4$  in all cases (H&H). Equation 4 accounts for the transition between strength and gravity regime, allowing a smooth transition between those extreme conditions.

The second scaling law considered is reported by Ivanov et al. (2001), (adapted from Schmidt & Housen 1987) (I&S hereinafter):

$$\frac{D}{d(\delta/\rho)^{0.26}v_{\perp}^{0.55}} = \frac{1.28}{[(D_{sg} + D)g]^{0.28}} \quad (5)$$

where  $D_{sg}$  represents the strength-gravity transition crater.  $D_{sg}$  has been set equal to 120 m and 30 m for the Moon and the Earth, respectively (Asphaug et al. 1996).

Finally, we have considered the scaling law used by Stuart & Binzel (2004) (adapted from Shoemaker et al. 1990) (S&S hereinafter):

$$D = 0.0224 \left( W \frac{\delta}{\rho} \right)^{0.294} \left( \frac{g_e}{g} \right)^{1/6} (\sin \alpha)^{2/3} \quad (6)$$

where,  $W$  is the impactor kinetic energy,  $g_e$  is the Earth gravity and  $\alpha$  is the impactor angle with respect to the surface (vertical impacts correspond to  $\alpha = \pi/2$ ). The numerical multiplicative factor takes into account the correction from transient to final crater dimension (Stuart & Binzel 2004). The crater size  $D$  reported in these formulas should be regarded as the size of the final crater. However, following Pike (1980), a correction for the transition between simple and complex craters has also been applied to all the scaling laws in the form of:

$$D = D \quad \text{if } D < D_{\star} \quad (7)$$

$$D = \frac{D^{1.18}}{D_{\star}^{0.18}} \quad \text{if } D > D_{\star} \quad (8)$$

where  $D_{\star}$  is the diameter of the transition from simple to complex crater<sup>2</sup>. All impacts are assumed to occur at the most probable impact angle, namely  $\pi/4$  with respect to the normal to the surface.

All the scaling laws assume that the density and the strength of the target are constant throughout the body. However, most target bodies are characterized by a layered structure, with a density increasing with depth. Therefore, in order to produce a better representation of the target density, we have computed the average density over a depth of about 10 times the radius of the projectile. This is because the size of the crater is -on average over different impact conditions- about a factor ten larger than the size of the impactor. In particular, in the case of the Moon we have assumed a 10-km layer of fractured silicates (megaregolith and heavily fractured anorthosites), on top of a bulk anorthositic crust in turn laying above a peridotitic mantle (see fig. 3). For the Earth (see fig. 3) we considered the following lithospheric structure (Anderson 2007): a 2 km thick layer of sedimentary rocks, a mainly granitoid upper-crust down to a depth of 20 km, a denser lower

<sup>2</sup> $D_{\star}$  has been set equal to 18 km and 4 km for the Moon and Earth, respectively (Ivanov et al. 2001).

crust down to 40 km, a peridotitic lithospheric mantle which is in turn characterized by an upper layer with an average density of  $3.2 \text{ g/cm}^3$  (up to 150 km), and a lower layer with a higher density ( $3.3 \text{ g/cm}^3$ ). The impactor density has been set to  $2.7 \text{ g/cm}^3$ . Regarding the strength, the value reported by Asphaug et al. (1996) for bulk silicates, namely  $Y_0 = 2 \times 10^8 \text{ dyne/cm}^2$  was used both for the Moon and Earth crusts. However, we assume a linear increase of the strength, from zero at the surface up to  $Y_0$  at the bottom of the heavily fractured layer for the Moon in order to take into account the cohesionless regolith layer on the surface and the underlying megaregolith and anorthosites which are likely characterized by a progressive decrease in fracture density with depth. A similar assumption was adopted also for the layer of sedimentary rocks on the Earth. The strength at the Earth's surface was set to  $0.3 \times 10^8 \text{ dyne/cm}^2$ . Following our description of the Moon crust, its upper layers are mainly made of highly fractured materials, which behave like cohesive soils. Therefore, we set a sharp transition in the scaling law, from cohesive soil in the case of small impactors to hard rock for larger ones, at a projectile size of  $1/20^{\text{th}}$  of the thickness of the heavily fractured silicate layer (i.e. 0.5 km). For the Earth only the hard rock scaling law was used since only rocky layers have been assumed at the surface.

### 3. The Model Production Function (MPF)

We have now all the necessary inputs for computing the cumulative crater size distribution (hereafter the Model Production Function, MPF) for the target bodies. Let  $\Phi(D)$  be the crater differential distribution, we may write:

$$\text{MPF}(D) = \int_D^\infty \Phi(\tilde{D}) d\tilde{D} \quad (9)$$

where  $\Phi$  can be expressed in terms of  $\phi$  and  $\mathcal{S}$  (see appendix for details). In figure 4 our lunar model production function is shown for different scaling laws along with the Neukum production function for the Moon (NPF). The NPF has been the traditional reference for dating purposes since the late 70s, with a few revisions in more recent times (Neukum 1983; Neukum et al. 2001). An alternative production function, the so-called HPF, has also been proposed by Hartmann et al. (1981).

A detailed comparison between these two production functions can be found in Neukum et al. (2001). For our purposes, we recall that the NPF shows an overall agreement with the HPF, even if some discrepancies are present. Nevertheless, as stated in Neukum et al. (2001), the NPF-based chronology represents the current best interpretation for the lunar cratering chronology. Moreover, since the NPF extends to a wider size range than the HPF, the former is more suitable for a thorough comparison with the MPF. For these reasons, here we provide detailed comparison between the MPF and the NPF. In the following paragraph, we briefly recall how the NPF has been derived.

There are several versions of the NPF. In this paper we refer to the *old* NPF (Neukum & Ivanov 1994) and to the *new* NPF (Neukum et al. 2001). In both cases, the underlying assumption is that the shape of the production function has been constant, with only the absolute number of craters changing over time. Therefore, the NPF was built by vertically re-scaling crater counts from areas with different ages, until they overlapped. The final curve was then expressed as a polynomial fit of the re-scaled data points. The strength of such procedure is that it is not model dependent because based on measured data. On the other hand this procedure, relying on the accuracy of the measurements in multiple overlapping regions, is particularly prone to severe error propagation, especially at the large diameter end. In addition, in some regions the cumulative distributions of craters can be altered by surface processes like sporadic magma effusions, ejecta from other craters etc. The subsequent effects of superposition of geological units of different ages, normally not recognizable on remote sensing images, can lead to mixed crater size distributions (Neukum & Horn 1976). Figure 4 clearly shows how the change of crater counting on single regions may alter the final shape of the NPF. In particular, the discrepancies between the old and the new NPF are due to an adjustment of the crater counts for Orientale Basin (Ivanov et al. 2001). A few considerations can be drawn from fig. 4. The first one is that different scaling laws produce differences on the MPF as large as a factor of ten for large craters. We find that the MPF produced with the S&S scaling law is not in good agreement with the NPF throughout the whole size range.

When applying the same scaling law to the observed NEO population, Stuart & Binzel (2004) found a better match to the new NPF for craters  $> 10$  km. This discrepancy is mainly due to the different value of the intrinsic probability that Stuart and Binzel used in their model (namely,  $1.50 \cdot 10^{-9} \text{ yr}^{-1}$ ). However, we believe the Bottke et al. determination of the intrinsic collision probability to be more accurate since it relies on a better treatment of the gravitational focusing effects (A. Morbidelli, pers. communication). The main difference between the H&H and the I&S scaling laws takes place at crater sizes smaller than 10 km. This can be traced back to our choice of using the cohesive soil scaling law for small crater sizes in the H&H scaling law which causes an inflection point in the MPF. This transition in the target's crustal properties produces an S-shaped feature in the MPF, which is qualitatively similar to the one found in the NPF. This finding would suggest that the observed S-shaped feature in the NPF is caused by physical properties of the target, rather than reflecting the shape of the size distribution of the impactors, as proposed by Werner et al. (2002) and Ivanov et al. (2002). Actually, a weak wavy feature in the relevant size range is present in the  $h_n(d)$  which, however, is smeared out when passing to the MPF. However, in order to finally assess this issue, a better estimate of the observed impactor size distribution for sizes  $< 0.1$  km is needed. It should also be mentioned that the detailed shape of the NPF somewhat depends on the fitting procedure used to construct the NPF itself, as shown by the mismatch between the old and new NPF for large craters.

In conclusion, despite of all the caveats mentioned, it is a remarkable result that the present MPF obtained with the H&H scaling law and the NPF (both new and old) are similar within a factor of two throughout the whole size range considered, that is from 0.01 km to a few hundred km. On the other hand, the S&S and I&S scaling laws fail to accurately reproduce the absolute number of craters per  $\text{km}^2$  per yr, with a maximum deviation of a factor of 10. The good agreement of the absolute density of craters per yr derived from the observations (either the NPF or the HPF) and the MPF with the H&H scaling law is therefore a clear indication that the latter scaling law is the more appropriate in describing the lunar crater-

ing. This agreement is particularly interesting, considering that the NPF and MPF are derived from completely independent methods: one being based on crater counting, and the other being the result of theoretical modeling. For these reasons, we decided to restrict the following analysis to the H&H scaling law. We refer to this MPF as to the *nominal model*.

### 3.1. The reliability of the nominal MPF

In this section we explore the effects that the various parameters involved in our model have on the nominal MPF described in the last section. In particular, we analyze the scaling law, the NEO size distribution and the assumed density and strength profiles.

The H&H scaling law depends on three parameters (namely  $k$ ,  $\nu$  and  $\mu$ ) which have been derived by best fit to laboratory data. We applied a variation of 10% around their nominal values, and computed the resulting MPF. It results that  $k$  and  $\nu$  have a negligible effect on the MPF. Changing  $\mu$  of  $\pm 10\%$ , the MPF shifts vertically of about a factor of  $\pm 2$ , respectively.

A detailed comparison of the modeled and observed NEO size distributions can be found in Bottke et al. (2005a,b). For our purposes, we notice that they basically overlap for  $d > 1.5$  km. For smaller impactor sizes, the situation is less clear since different surveys produce slightly different observed distributions. Anyway, we can safely state that we have a maximum deviation between the observations and the model distributions of about a factor of 1.8 (being the observations lower than the model).

The scaling law is weakly dependent on the density, so a change in the numerical values affects the MPF in a negligible way. Notice also that craters larger than about 0.1-0.2 km form in gravity regime, hence the rock strength is not important at those sizes. For smaller sizes, the shape of the MPF may depend on the local strength. The density and strength profiles adopted in this work are meant to be average profiles for the Moon. Local variations to the mean values may slightly change the MPF at small crater sizes.

A more important parameter is the assumed depth for the transition from cohesive to hard rock scaling law. A variation in this value causes a shift of

the inflection point in the MPF within the range  $1 < D < 10$  km.

#### 4. A new chronology for the Moon

The MPF can be used as a reference to develop the lunar chronology. For this purpose, we used literature crater counts from regions with known radiometric ages as calibration regions. A list of the regions used is reported in table 1.

In order to obtain the lunar chronology, we first assumed that the MPF shape remained constant over time. For each calibration region we determined the proportionality factor which gave the best fit to the data by minimizing the  $\chi^2$ . Finally, we determined the crater cumulative number at 1 km ( $N_1$ ). The fitting procedure used is particularly important, as it directly affects the chronology. For this reason, we performed several tests in order to assess its stability. A major aspect consisted in choosing the weights given to the measured data points. It is common practice in crater counting to assign each data point an error bar corresponding to the square root of the number of counts, under the assumption that the measurements follow a Poisson distribution. However, in the case in which significant systematic effects are present, this procedure leads to underestimate the total error. This problem is particularly evident when dealing with small craters that are at the limit of the image resolution. Because of their large number, the statistical error for these craters is comparatively small. On the other hand, due to the difficulty of positively identifying craters at the limit of the resolution, these measurements could be affected by a significant bias. This effect may affect the  $N_1$  values up to a factor of 3-4 in some regions and consequently have a non negligible effect on the chronology. After several tests, we decided to use the following weights:

$$\sigma_t^2 = N + \kappa N^2 \quad (10)$$

where  $\kappa$  was set to 0.5. In this way, the total error ( $\sigma_t$ ) for points with very low statistical  $\sigma$  were increased, while those with large statistical error (i.e. low number of craters) were basically left unchanged.

In order to validate this procedure, we applied it to the old NPF, being able to reproduce the

Neukum & Ivanov (1994) results within their error bars<sup>3</sup>.

#### 4.1. Moon cratering

In this section we present the results of the fits applied to the regions used to calibrate the lunar chronology (see tab. 1). The fitting procedure was successful for most of the regions. In several cases a very good fit was achieved through the measured range of the cumulative distributions, indicating an overall agreement between the shape of the MPF and the data. However, some discrepancies occurred for the highlands (for  $D > 100$  km), Mare Crisum and Mare Tranquillitatis. In the case of the highlands (see fig. 5), the discrepancy seems to suggest a different shape of the impactor size distribution in the past, with a larger fraction of medium-to-large impactors (see section 5 for further details). In the case of Mare Crisum and Mare Tranquillitatis regional phenomena can be responsible for the observed deviations. In particular, in both cases several consecutive magma flows have partially covered the population of small craters, affecting the observed cumulative distribution (Neukum & Horn 1976; Boyce et al. 1977). Indeed the absolute radiometric ages derived from A11 samples (Mare Tranquillitatis), span from 3.5 to 3.85 Gyr, whereas the ages of the Luna 24 basalts (Mare Crisium) are clustered into at least three different peaks at 2.5, 3.3, 3.6 Gyr, respectively (Birck & Allègre 1978; Stöffler & Ryder 2001; Fernandes & Burgess 2005). In presence of such surface phenomena, the fit must be constrained on the basis of geological considerations, as the automatic fit may be misleading. In particular, as formerly suggested by Neukum & Horn (1976), the crater size-frequency distribution derived from these regions leads to a composite curve in which smaller craters reflect the younger radiometric ages, while the larger ones correspond to older ages. Thus, for Mare Tranquillitatis we forced the MPF to overlap the cumulative curve at 0.5 km for the age of 3.55 Gyr (referred to as *young*), and at 0.9 km for the age of 3.72 Gyr (referred to as *old*). Similar considerations hold also for Mare Crisum where the MPF

<sup>3</sup>Here we used the old NPF instead of the new NPF because even the latest chronology by Neukum et al. (2001) uses the old NPF.

was fitted to craters with diameters in the range 1 to 2 km (details on the fit of the calibration regions are reported in the online material).

Another effect influencing the accuracy of the crater statistics is the possible presence of secondary craters. Even though authors publishing crater counts pay particular attention to the identification and rejection of secondary craters, in some cases confusion with primary craters is difficult to avoid. According to Ivanov (2006), secondaries are likely negligible on young regions because they did not have the time to accumulate in large numbers. On the other hand, older regions, namely the highlands and maria, may show secondary craters caused by subsequent large impacts (Wilhelms 1976). Nevertheless, Neukum & Ivanov (1994) concluded that the secondaries are likely not relevant. For the present analysis, we assumed that the observed crater cumulative distributions are resulting from the primary flux of impactors.

#### 4.2. Earth cratering

Cratering studies are much more difficult on the Earth than on the Moon, due to strong resurfacing processes and consequent alteration of the crater morphologies. Nevertheless, Earth craters are important because they can be studied in detail and precisely dated. Therefore they can be used to further constrain the flux of impactors, in particular for young ages, that are scarcely represented in lunar data. In this work two data sets of terrestrial craters have been considered. The first one consists of all large craters ( $D > 20$  km) found on the North American and Euroasiatic cratons, as presented by Grieve & Dence (1979) (updated with few new findings from the Earth Impact database<sup>4</sup>). Following Grieve & Dence (1979), we have adopted for these two cratons an age of 0.375 Gyr. Some sectors of both cratons were probably exposed to the meteoroid flux already from the early Ordovician (0.450 Gyr), whereas others only from 0.300 Gyr ago (Grieve & Dence 1979). The choice of 0.375 Gyr is further supported by the age of the older craters that, with only few exceptions, are around this value.

The second data set represents a subset of the first one, including only craters with radiometric

ages less than 0.120 Gyr. This choice has been made following Grieve (1993), in order to overcome biases due to erosion and burial of craters on the Earth's surface. Both cumulative distributions were fitted using our Earth MPF, and the obtained  $N_1$  was rescaled to the lunar case by considering the gravitational focusing and the different relationships between impactor and crater size on the two bodies (see fig. 6). The resulting values for  $N_1$  are shown in tab. 1, with more details supplied in the online material.

#### 4.3. MPF chronology

The lunar chronology has been developed on the basis of the relationship between the derived  $N_1$  values and the absolute ages. However, this task is not trivial since only 18 measurements are available, 12 of which are older than 3 Gyr. Moreover, the region from 1 Gyr to 3 Gyr lacks completely in data points. Therefore a very accurate chronology cannot be expected, in particular for ages younger than 3 Gyr. In this work the radiometric ages proposed by Stöffler & Ryder (2001) were used.

In order to describe the lunar chronology, Neukum (1983) suggested the following approximation:

$$N_1 = a(e^{bt} - 1) + ct. \quad (11)$$

This function assumes a linear relationship between  $N_1$  and the age ( $t$ ) for  $bt \ll 1$ , while for  $bt \gg 1$   $N_1$  increases exponentially. Although this is a rather simple description of the data, it accurately fits the data points in the Neukum chronology. We fitted the same function to our MPF-based data points, with the results shown in fig. 7. The derived coefficients are:  $a = 1.23 \times 10^{-15}$ ,  $b = 7.85$ ,  $c = 1.30 \times 10^{-3}$ . For comparison, Neukum & Ivanov (1994) obtained:  $a = 5.44 \times 10^{-14}$ ,  $b = 6.93$ ,  $c = 8.38 \times 10^{-4}$ , which are quite similar to our result<sup>5</sup>. The Neukum & Ivanov

<sup>5</sup>As previously discussed, old regions with cumulative counting extending to sub-km sizes may be affected by secondaries. These regions are: Descartes Formation, Mare Imbrium, Mare Fecunditatis, Taurus Littrow Mare, Mare Tranquillitatis. Therefore we also performed a best fit excluding these regions. The resulting coefficients are  $a = 3.07 \times 10^{-15}$ ,  $b = 7.63$ ,  $c = 1.33 \times 10^{-3}$ , and the resulting chronology curve is basically overimposed to the one obtained using all the regions. Therefore the secondary craters -if presents in the cumulative distributions- do not affect the chronology.

<sup>4</sup><http://www.unb.ca/passc/ImpactDatabase/>.



(1994) chronology curve is also plotted in fig. 7. While the derived best fit is in overall agreement with the nominal MPF-based data points, there are some deviations that mainly concern young data points, which lie systematically above the best fit curve. It is remarkable that in our chronology, the proposed equation fits well all the points older than Copernicus (which was an outlier in the chronology of Neukum & Ivanov 1994), while it underestimates -by a factor of 2- all the points younger than Copernicus (see fig. 7).

#### 4.4. Non-constant flux in recent times?

As mentioned, the MPF-based chronology is reasonably in agreement with that derived from the NPF. The discrepancies observed for young regions could be due to uncertainties involved in our model. In particular, a concern regards the slope of the impactor cumulative size distribution for small dimensions which is poorly constrained by observations. Errors in the slope in this size range may result in inaccurate estimates of  $N_1$  for the young lunar regions. The slope of the NEO model for impactor diameters smaller than 0.1 km (which roughly corresponds to 1 km crater size) is -2.6, which becomes a slope of -3.1 in the MPF. This slope is very similar to that of the NPF for the same size range, which is equal to -3.2. This slight difference in slope can account for half of the observed difference between our and Neukum's chronology. We underline that such slope variations may affect the Cone, Tycho and North ray craters, but not the terrestrial crater counts since they have  $D > 20$  km. Therefore it is remarkable that terrestrial craters lie on the same linear trend of the young lunar data points (fig. 7, left panel). The NEO population model adopted here is in overall agreement with the available observed data (see fig. 16 of Bottke et al. 2005b). For small dimensions, however, the real NEOs size distribution is poorly known. The only observational constraints are the small fireballs (Halliday et al. 1996) and bolides (Brown et al. 2002) detected in the Earth's atmosphere. A careful check at fig. 16 of Bottke et al. (2005b) shows that the NEO population model slightly overestimates -by a factor of about 1.5- the predicted number of NEOs from bolide data. This occurs for the impactor size range responsible for the cratering observed for the Cone, North Ray and Tycho craters. Based on the

data presently available, it is very difficult to understand whether this difference is real or rather due to the involved uncertainties. Nevertheless, if we maintain the present number of NEOs at  $d = 1$  km, we obtain that the  $N_1$  values corresponding to the younger lunar regions would be further increased.

Other possible sources of uncertainties may arise from the scaling law. Nevertheless, variations in the parameters produce a vertical shift of the MPF and not a change of the shape, therefore this shift alone cannot affect the determination of  $N_1$  values. The only way to obtain a change in the  $N_1$  values with respect to the nominal model, is to introduce a slope variation in the MPF for  $D < 1$  km. This would be the case, if the inflection point would slide below  $D \sim 1$  km. This would imply a very low thickness for the fractured layers which seems improbable, according to our understanding of the lunar crust. Nevertheless, if this would be the case,  $N_1$  for the young lunar regions would be further increased.

It is also possible that the MPF-based  $N_1$  values are accurate, and the simple relationship proposed by Neukum (1983); Neukum & Ivanov (1994) is not adequate to describe the data. This would be the case, for example, if the impactor flux had not been constant during the past  $\sim 3$  Gyr. Due to the lack of data points in the range 1-3 Gyr, we are not able to study in detail possible variations in the flux. However, fig. 7 seems to suggest that a recent phase (age  $< 0.4$  Gyr) characterized by a constant impactor flux was preceded by a phase (between 0.8 and 3 Gyr) with a lower and nearly constant impact rate. A single event placed around 0.4 Gyr ago and lasting for 0.2-0.3 Gyr that would increase the impactor flux by a factor 2-3 would explain the observed data. Such a recent change in impactor flux would also have affected the older regions, but here the relative increase in the number of craters would be very low compared to the accumulation of craters over 3 Gyr or more, hence this effect would be negligible. This scenario is qualitatively in agreement with the recent suggestion of an increase in the number of impactors in the inner Solar System due to the formation of dynamical families -as a results of catastrophic disruption of asteroids- in the main belt (Nesvorný et al. 2007; Bottke et al. 2007). In particular, the Baptistina and Flora families are estimated to have

formed about 140 Myr and 500 Myr ago, respectively. Their proximity to the resonances led to an increase in the number of the NEO population, starting few tens of Myr after their formation, as a consequence of the Yarkowsky-effect-driven decay of the semimajor axis. In the case of Baptistina the maximum flux was reached about 60 Myr after its formation (i.e. 80 Myr ago). Therefore this flux may have affected the Cone, North Ray and Tycho craters counting<sup>6</sup>, and also the young terrestrial craters.

Concerning the formation of Flora, similar considerations may hold. In addition, the Flora family has been connected to the spike in the infall of L-chondrite meteorites that occurred about 470 Myr ago (Bogard 1995). A similar spike has also been detected in the lunar glass spherules and -to a lesser extent- in lunar impact clasts (Culler et al. 2000; Cohen et al. 2005). These spikes may have affected mostly the terrestrial cratering and the Copernicus counting. Although such enhancement of the flux was probably formed by sub-km impactors (Hartmann et al. 2007), the spike recorded in the lunar melt clasts implies also the existence of a number of km-sized impactors. This enhancement in the km-sized impactors may explain why the Earth cratering for  $D > 20$  km seems not to be depleted by erosion processes (fig. 7, left panel), as expected (Grieve 1993).

#### 4.5. On the early flux

One of the major -and mostly debated- open issues is related to the cratering rate in the early times after the formation of the Moon. Arguments have been proposed in favor of a rapid and smooth decrease in the impact rate from the formation of the Moon till about 3.5 Gyr ago (Hartmann et al. 1981; Neukum 1983), followed by a constant impact rate (Neukum 1983; Neukum & Ivanov 1994). On the other hand, studies of impact melts led some researchers (e.g. Ryder 1990; Stöffler & Ryder 2001; Cohen et al. 2000) to support the idea of an intense lunar bombardment about 3.9 Gyr ago which lasted some 100-200 Myr. From a dynamical point of view, such short phase of intense bombardment has been

<sup>6</sup>See the discussion in Bottke et al. (2007) about the probability of Tycho itself being formed by an impact with a Baptistina fragment.

recently explained in the more general context of the early stages of the evolution of the Solar System (Gomes et al. 2005). This scenario has also found some observational evidence in the work of Strom et al. (2005).

Despite these works, the LHB hypothesis has not found an unanimous consensus yet. For instance, Hartmann et al. (2007) raised doubts about the interpretation of lunar melts and glasses data; while Neukum & Ivanov (1994) argued against the LHB on the basis of the smooth behavior of their lunar chronology curve.

If the intense LHB did take place, it should have left some traces in the chronology curve, which therefore could be used to obtain constraints on the early stages of the cratering. Unfortunately, there are only 5 measured regions having ages older than 3.85 Gyr, and therefore it is not easy to draw firm conclusions. One of the most important regions is the Nectaris Basin. Neukum & Ivanov (1994) used a radiometric age of 4.1 Gyr. The resulting best fit for the lunar chronology curve is therefore very close to all the old regions (within errors) and has a smooth behavior in early times, reflecting a possible smooth decay in the impact rate (see fig. 7). However, using the new estimate of 3.92 Gyr for Nectaris Basin proposed by Stöffler & Ryder (2001) this point moves considerably far from the best fit (this is the age we used in our chronology). This results in a change of the slope of the chronology curve, which in turn is in favor of the LHB. We underline that in the present analysis we used the present NEO size distribution. However, it is very likely that at the time of the LHB the impactor size distribution had a different shape. At the present stage of knowledge a firm conclusion from the chronology curve cannot be obtained. Nevertheless, we will add few considerations on this important point in the next section.

## 5. A time-dependent MPF

In this section we develop a time-dependent MPF. In doing so, we clearly show the versatility of our approach, as opposed to the conventional methods (e.g. the NPF), where the production function is generally assumed to be constant over time. Modeling a time-dependent MPF is quite complex, and in this section we will only pose the basis of the problem, deferring thorough investiga-

tions to a further analysis. In general terms, there are two possible reasons for such time-dependent behavior: The first one is related to a non stationary flux<sup>7</sup>,  $\phi(d, v, t)$ ; the second one to crater erasing processes.

A motivation for studying the non stationary flux is provided by the dynamical processes responsible for the flux. In early times (just after the formation of the terrestrial planets and the Moon, some 4.5 Gyr ago) the inner Solar System was still populated by the leftover planetesimals, which were rapidly (10-100 Myr) cleared-up by the latest stages of the accretion process. A second source of impactors was represented by the highly perturbed bodies (e.g. through the *sweeping resonance* mechanism) due to the formation and migration of Jupiter. At the present time, the flux is mainly sustained by the slow decay of MBAs into the resonances. All these three stages have their own characteristic  $\phi(d, v)$ . For sake of simplicity, here we focus on the last two mechanisms. The second process is size dependent, while the first one is not, therefore the shape of the impactor size distribution changes over time. On the other hand, the impactor velocity distribution is expected to remain approximately constant over time, as in both cases the transport mechanism to the NEO space is the same. Therefore we may write  $\phi(d, v, t) = h(d, t)f(d, v)$ .

The crater erasing on large bodies depends mainly on two major effects: the superposition of craters and the local jolting (O'Brien et al. 2006). The first one basically accounts for the overlapping of craters as the surface crater density increases. The second one considers the erasing of craters due to local seismic jolting triggered by the formation of large craters. Both effects can be modeled by considering a variation in the number of craters in a given size bin (O'Brien et al. 2006). Let  $\mathcal{E}$  be the ratio between the actual number of craters considering the erasing and the total number neglecting the erasing, we can write:

$$\text{MPF}(D, t) = \int_D^\infty \Phi(\tilde{D}, t)\mathcal{E}(\tilde{D}, t) d\tilde{D} \quad (12)$$

<sup>7</sup>We stress once again that in our approach what is relevant is the shape of the impactor size and velocity distributions, since the absolute calibration of the model is done by the reference lunar regions.

where setting  $t = 0$  and  $\mathcal{E} = 1$  reduces to the MPF used in previous sections (see appendix for further details). Here we limit ourselves to considering these effects separately. Let us consider first the crater erasing mechanism, assuming  $\phi \equiv \phi(d, v, 0)$  as in previous sections. The results are shown in fig. 8. It is clear that as the age increases the MPF becomes flatter for small dimensions. This is the well-known saturation process of heavily cratered surfaces. This affects the derived  $N_1$  values. To study possible variations in the rate of impacts over time, we adopted the following procedure: first the cumulative distributions for the calibration regions were fitted with the MPF corrected for the erasing, then the obtained  $N_1$  was rescaled to the total number of craters that occurred in the region (i.e. the actual number of impactors). In fig. 9 the effects of the erasing on the chronology are shown. Although the erasing considerably changes the MPF for the old ages (see fig. 8), its effects on the chronology are not important.

Let us now deal with changes in the impactor size distribution and no erasing ( $\mathcal{E} \equiv 1$ ). Following the previous discussion, we assumed that before the end of the LHB ( $\sim 3.8$  Gyr ago) the size distribution  $h(d)$  resembled closely that of the main belt<sup>8</sup> ( $h_m$ ), while afterwards it becomes similar to the present one, that is  $h_n$ . This assumption is also encouraged by the observation that  $h_m$  provides a much better fit to the crater distribution of the highlands and Nectaris Basin than  $h_n$  does (see online material). With respect to the previous analysis (see fig. 7), the only difference regards two data points, namely the highlands and Nectaris Basin. For both regions we obtain a lower  $N_1$  value, with the reduction being more pronounced for the highlands. This results in a net change in the slope of the chronology in the two oldest points, suggesting a change in the rate of impactors. Therefore, if the MBA size distribution is used for earlier times on the basis of the improved fit with both the highlands and Nectaris Basin, the chronology plot would suggest the existence of the LHB. These conclusions are weakly affected by the uncertainties in the model (size distribution, scaling law etc.) because the MPF is

<sup>8</sup>For sake of simplicity, we used the present MBA size distribution although it may have had a different shape in the past (Bottke et al. 2005a,b).

well defined for the large crater sizes relevant in this context.

## 6. Mercury’s chronology

The impactor size and velocity distributions for Mercury have been computed in a similar way as done for the Moon (figs 10, 11). We assumed density and strength profiles similar to those adopted for the Moon. The resulting MPF is shown in fig. 12 (right panel), along with the overplot of the NPF for Mercury (Neukum et al. 2001b). The two production functions nicely overlap at the extremes, that is for  $D < 0.3$  km and  $D > 40$  km. Inside this range, however, the two curves are quite different, with a maximum deviation of nearly a factor of 5 at  $D \sim 3$  km (fig. 12, left panel). The exact behavior of the MPF in this range depends on the assumptions on the transition in the scaling law between cohesive soil and rock (see discussion in sect. 2.2). Nevertheless, whatever reasonable choice is made for the scaling law parameters, our MPF is remarkably different from the NPF in this range.

As an example, we report here our age determination of the Chekhov basin. Crater counting was performed on the total ejecta blanket, over an area exceeding  $4 \cdot 10^4$  km<sup>2</sup>. According to the analysis of Neukum et al. (2001b), Chekhov basin has a derived age of 4.05 Gyr, which makes it one of the oldest regions on Mercury. In fig. 13 we report our MPF-based age estimate, obtained considering different scenarios, namely using the NEO and MBA size distributions. In the nominal case (i.e.  $\text{MPF}=\text{MPF}(D, 0)$ ;  $\mathcal{E} = 1$ ), we obtain an age of 3.94 Gyr, which is slightly younger than that found by Neukum et al. (2001b). The corresponding  $\chi^2$  of the best fit is 0.8. Note that, in comparison to the NPF ( $\chi^2=1.5$ ), the MPF more closely fits the observed crater cumulative distribution. When considering also the crater erasing, the age becomes 4.05 Gyr ( $\chi^2=0.6$ ), and the shape of the MPF is basically unchanged. In the case of the MBA size distribution and no erasing, we obtain 3.97 Gyr ( $\chi^2=0.6$ ). Notice that in the case of MBA, if we include crater erasing the MPF reaches the saturation prior to achieving the best fit, therefore it is not possible to derive a precise age estimate. In conclusion, the MPF shows a better fit to the data points than the NPF. How-

ever, due to the measurement errors and to the limited crater size range observed, it is not possible to conclude whether the NEO or the MBA size distribution is more suitable for fitting the Chekhov basin.

## 7. Conclusions

In this paper a new model for the chronology of planetary surfaces in the inner Solar System has been introduced and applied to the Moon and Mercury. Concerning the Moon, the main findings are the following:

- The nominal MPF differs from the NPF for less than a factor of 2 throughout the observed range of dimensions. A similar degree of agreement is obtained for the chronology;
- Despite the good agreement between MPF and NPF, there is a systematic misfit of the assumed linear branch of the chronology function with the data points for ages more recent than about 0.4 Gyr. It is remarkable that the Earth craters (which have  $D > 20$  km) are aligned with the Tycho, Cone and North Ray craters (having  $D < 0.4$  km). Although the misfit may be partially due to the uncertainties present in the model, other causes, such as for instance a non-constant flux in recent times due to the formation of MB families (like Baptistina and Flora) might be possible;
- The MPF was computed for two different impactor size distributions, namely the present NEO and MBA populations. In this way we were able to study whether the cratering production function changed over time. Both the NEO and MBA-based MPFs are able to fit the cumulative distributions having ages  $< 3.9$  Gyr. This is mainly due to the fact that such regions have craters smaller than  $\sim 10$  km, where the MPFs are very similar. On the other hand, the oldest regions (highlands 4.35 Gyr; Nectaris Basin 3.92 Gyr) are best fitted using the MBA size distribution. This suggests that the impactor size distribution around 4 Gyr ago resembled the present MBA distribution, while today it is closer to the present

NEO size distribution. Alternatively, it is also possible that comets had in the past a non negligible contribution. This point deserves a specific analysis and will be subject of a future work;

Concerning Mercury, the MPF differs from the NPF in the size range from 0.3 km to 40 km. The maximum difference -of about a factor of 5- occurs at  $\sim 3$  km. This discrepancy is therefore potentially important for dating purposes, in particular when measurements for small craters will become available (e.g. from MESSENGER and BepiColombo). Outside this range, the NPF and MPF are very similar. We show the results of our model for the case of the Chekhov basin. In the nominal case (MPF( $D, 0$ ),  $\mathcal{E} = 1$ ) we obtained the age of 3.95 Gyr, which compares to the 4.05 Gyr of Neukum et al. (2001b).

We are grateful to A. Morbidelli for helpful discussions and for providing us with the results of the orbital integrations. We are also grateful to R. Wagner for providing us with the original lunar cumulative distributions. Thanks to G. Neukum for helpful discussion and suggestions. We also thank W. Bottke for providing us with the size distribution of NEOs and MBAs. Finally, thanks to D. De Niem and G.F. Gronchi for helpful discussions.

### A. The Model Production Function

The cumulative distribution of craters (the so-called *production function*) can be evaluated starting from the differential distribution of the incoming flux, namely  $\phi(d, v, t)$ . Here we consider the general problem of a non stationary flux, therefore the time dependence of the function  $\phi$ . Each impact produces a crater, with a size specified by the scaling law,  $D = \mathcal{S}(d, v, \vec{p})$ . Let  $\Phi(D)$  be the differential distribution of craters, namely the number of craters per unit of crater size per unit surface. Such distribution is obtained by integrating the differential distribution of impactors over the one-dimensional domain specified by the scaling law, namely  $\gamma_D : \mathcal{S}(d, v, \vec{p}) = D$ . Let  $\sigma$  be a parameter along the curve  $\gamma_D$ , we finally have:

$$\Phi(D, t) = \int \phi(\gamma_D(\sigma), t) \left\| \frac{d\gamma_D}{d\sigma}(\sigma) \right\| d\sigma \quad (\text{A1})$$

In the presence of erasing processes, the actual number of measured craters in any given size bin  $dD$  is not equal to the number of impactors. Let  $\mathcal{E}(D, t)$  be the ratio of the final number of crater erasing included, with the total number (i.e. erasing excluded), we finally obtain:

$$\text{MPF}(D, t) = \int_D^\infty \Phi(\tilde{D}, t) \mathcal{E}(\tilde{D}, t) d\tilde{D} \quad (\text{A2})$$

Following the work of O'Brien et al. (2006), the function  $\mathcal{E}$  can be expressed as

$$\mathcal{E}(D, t) = \frac{1 - e^{-A}}{A} \quad (\text{A3})$$

where  $A$  is the total effective area of craters accumulated per unit area. Therefore  $A$  depends on the age since older regions have a large number of craters accumulated and hence a larger  $A$  with respect to younger regions.  $A$  also depends on crater diameter since small craters are more frequent than larger ones. As a results, the counting of small craters on old regions are strongly affected by the erasing (see fig. 8). In calculating  $A$ , we considered the superposition of craters and the local jolting, and neglected global jolting and cumulative effects of seismic shaking, since they are not relevant for large bodies like the terrestrial planets. The parameters involved in the estimate of  $A$  have been derived from O'Brien et al. (2006). The implementation of the erasing processes in our code has been tested accurately using asteroid crater counting (Gaspra, Ida, etc). Our results agree with those published. Nevertheless, the purpose of the present analysis is simply to show the first-order effects of the erasing, and a detailed evaluation of the erasing on planetary-sized bodies is left for further analysis.

TABLE 1  
DESCRIPTION OF THE LUNAR AND TERRESTRIAL CALIBRATION REGIONS USED IN THIS WORK.

Region	$N_1$ (NEO) <sup>†</sup> ( $\text{km}^{-2}$ )	$N_1$ (MBA) <sup>†</sup> ( $\text{km}^{-2}$ )	Age <sup>‡</sup> (Gyr)
Highlands <sup>a</sup>	$7.851 \cdot 10^{-1}$	$2.018 \cdot 10^{-1}$	4.35
Nectaris Basin	$1.327 \cdot 10^{-1}$	$6.648 \cdot 10^{-2}$	3.92
Descartes Formation <sup>b,s</sup>	$2.490 \cdot 10^{-2}$	$2.509 \cdot 10^{-2}$	3.92
Imbrium Apennines <sup>c</sup>	$1.968 \cdot 10^{-2}$	$1.931 \cdot 10^{-2}$	3.85
Fra Mauro Formation	$2.595 \cdot 10^{-2}$	$2.672 \cdot 10^{-2}$	3.85
Mare Tranquillitatis (old) <sup>d,s</sup>	$1.836 \cdot 10^{-2}$	$1.832 \cdot 10^{-2}$	3.80
Taurus Littrow Mare <sup>s</sup>	$1.579 \cdot 10^{-2}$	$1.585 \cdot 10^{-2}$	3.70
Mare Tranquillitatis (young) <sup>d,s</sup>	$9.300 \cdot 10^{-3}$	$9.357 \cdot 10^{-3}$	3.58
Mare Fecunditatis <sup>s</sup>	$3.234 \cdot 10^{-3}$	$3.257 \cdot 10^{-3}$	3.41
Mare Imbrium <sup>s</sup>	$5.468 \cdot 10^{-3}$	$5.526 \cdot 10^{-3}$	3.30
Mare Crisium	$2.335 \cdot 10^{-3}$	$2.377 \cdot 10^{-3}$	3.22
Oceanus Procellarum	$3.683 \cdot 10^{-3}$	$3.695 \cdot 10^{-3}$	3.15
Copernicus Crater (cont. ejecta) <sup>e</sup>	$1.321 \cdot 10^{-3}$	$1.337 \cdot 10^{-3}$	0.80
Copernicus Crater (crater floor) <sup>e</sup>	$1.348 \cdot 10^{-3}$	$1.343 \cdot 10^{-3}$	0.80
Terrestrial Phanerozoic craters <sup>f</sup>	$1.267 \cdot 10^{-3}$	$7.655 \cdot 10^{-4}$	0.375
Terrestrial Phanerozoic craters (young) <sup>g</sup>	$3.835 \cdot 10^{-4}$	$2.195 \cdot 10^{-4}$	0.120
Tycho crater (cont. ejecta) <sup>h</sup>	$3.391 \cdot 10^{-4}$	$3.401 \cdot 10^{-4}$	0.109
Tycho crater (cont. ejecta) <sup>i</sup>	$1.644 \cdot 10^{-4}$	$1.712 \cdot 10^{-4}$	0.109
North Ray crater <sup>l</sup>	$1.389 \cdot 10^{-4}$	$1.421 \cdot 10^{-4}$	0.053
Cone Crater <sup>l</sup>	$6.970 \cdot 10^{-5}$	$7.131 \cdot 10^{-5}$	0.025

NOTE.—Where not explicitly quoted, the data are from Neukum (1983) and references therein. The plots showing the fits of the calibration regions are reported in the online material.

<sup>†</sup>The derived  $N_1$  values both using the NEO and MBA size distributions.

<sup>‡</sup>Radiometric ages for the lunar regions are from table VI of Stöffler & Ryder (2001). The ages of the terrestrial craters are from Grieve & Dence (1979).

<sup>a</sup>All craters and basins.

<sup>b</sup>The counting for Descartes Formation is limited to dimensions smaller than 1.2 km, while that used in Neukum (1983) extends to larger sizes.

<sup>c</sup>The crater counting for Imbrium Apennines (used in this work) is a sub sample of the crater counting from Imbrium Basin, used by Neukum (1983).

<sup>d</sup>Original data from Greeley & Gault (1970).

<sup>e</sup>For the Copernicus crater we have two distinct measurements corresponding to the crater floor and the continuous ejecta blanket. In fig. 31 of Neukum (1983), these sets were probably merged into a single distribution. We decided to keep these two sets separate, and to provide individual fits (see fig. 7 and the online material).

<sup>f</sup>Terrestrial Phanerozoic craters are derived from Grieve & Dence (1979), and updated according to the Earth Impact Database (<http://www.unb.ca/passc/ImpactDatabase/>). Only large craters ( $D > 20$  km) on the North American and Euroasian cratons have been considered. For sake of completeness we report the list of craters used. In the North American craton: Beaverhead, Carswell, Charlevoix, Clearwater East, Clearwater West, Haughton, Manicouagan, Manson, Mistastin, Presquile, Saint Martin, Slate Islands, Steen River, Sudbury. In the Eurasian craton: Boltysh, Kamensk, Keurusselka, Lappajarvi, Puchezh-Katunki, Siljan.

<sup>g</sup>Only large ( $D > 20$  km) and young ( $< 120$  Myr) terrestrial craters. They are: Carswell, Haughton, Manson, Mistastin, Steen River, Boltysh, Kamensk, Lappajarvi.

<sup>h,i</sup>Two distinct measurements were available for the Tycho crater. Both correspond to the continuous ejecta: in (h) small craters were counted, while in (i) large craters were counted. In fig. 31 of Neukum (1983) these files were merged into a single distribution. We decided to keep these two sets separate, and to provide individual fits (see fig. 7). Notice that Neukum (1983), also reports 4 measured points in the range 0.5-1.1 km that were not available to us.

<sup>l</sup>Original data from Moore et al. (1980).

<sup>s</sup>These are relatively old regions having crater counting extending to small sizes ( $< 1$  km) and thus potentially affected by secondary craters. In order to check whether these regions affect the final MPF-based chronology, we also performed a best fit excluding these points. The results of the fit is basically unchanged (see text for further details.)



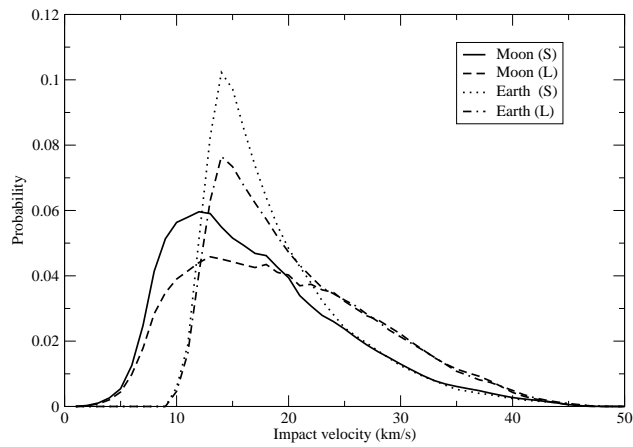


Fig. 1.— Distributions of impact velocities on the Moon and on the Earth, for two different impactor sizes. The smallest (S) and largest (L) impactor sizes used in these simulations are 0.1 m and 72 km, respectively. The average impact velocities are 18.6 and 20.0 km/s, respectively. Notice that these average impact velocities are slightly lower than those used by Neukum & Ivanov (1994), after applying the correction for the average impacting angle of  $\pi/4$ . The distributions are quite spread and therefore a large number of impacts occur at velocities considerably different from the average, thus affecting the final crater distribution (see text).

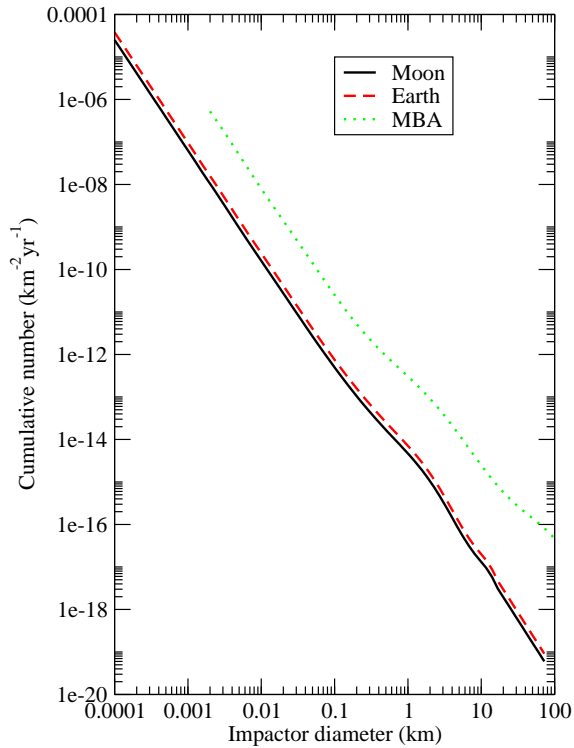


Fig. 2.— Model cumulative size distributions of impactors on the Moon and on the Earth (after Bottke et al. 2002). An arbitrarily rescaled MBA cumulative distribution (after Bottke et al. 2005a) is also shown for comparison. The main belt distribution shows an S-shaped feature in the 0.2-2 km size range. Also the NEO distribution shows a qualitatively similar feature. The two distributions, however, have quantitatively different shapes, due to selection mechanisms taking place during the dynamical transport from the main belt to the near-Earth space.

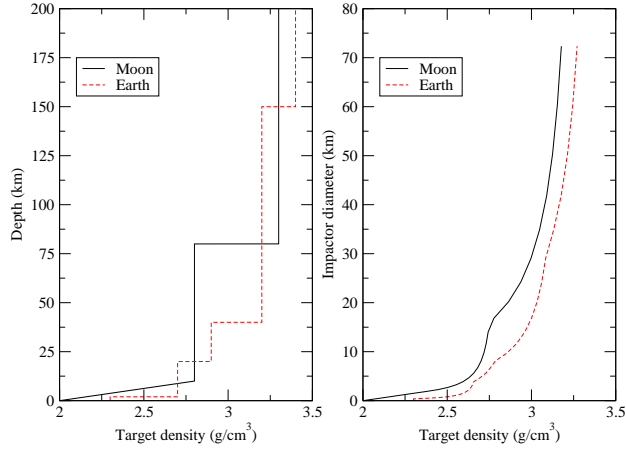


Fig. 3.— Assumed density profiles for the Moon and the Earth. Left panel: lunar and terrestrial density profiles vs depth. Right panel: average density vs impactor size. The average density has been obtained by averaging the density up to a depth of  $10\times$  the impactor radius. A similar consideration holds for the strength (see text for details).

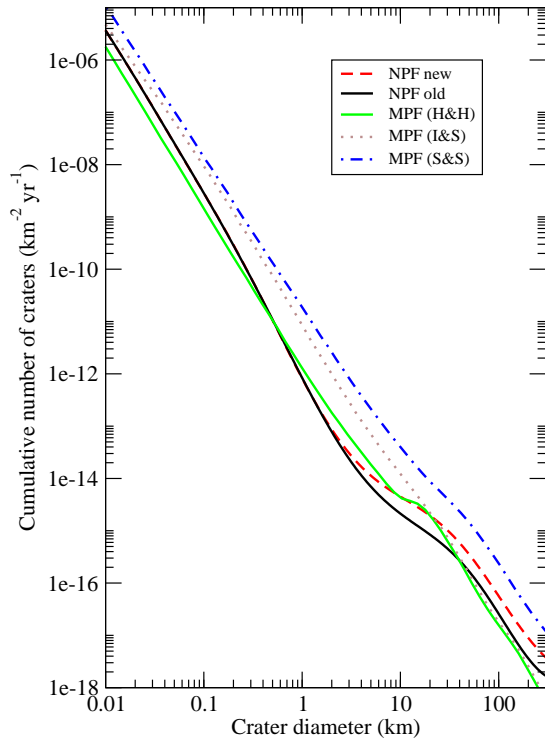


Fig. 4.— Comparison of the MPF obtained with different scaling laws, indicated by H&H, I&S, S&S (see section 2.2 for details). The old and new NPFs are also shown.

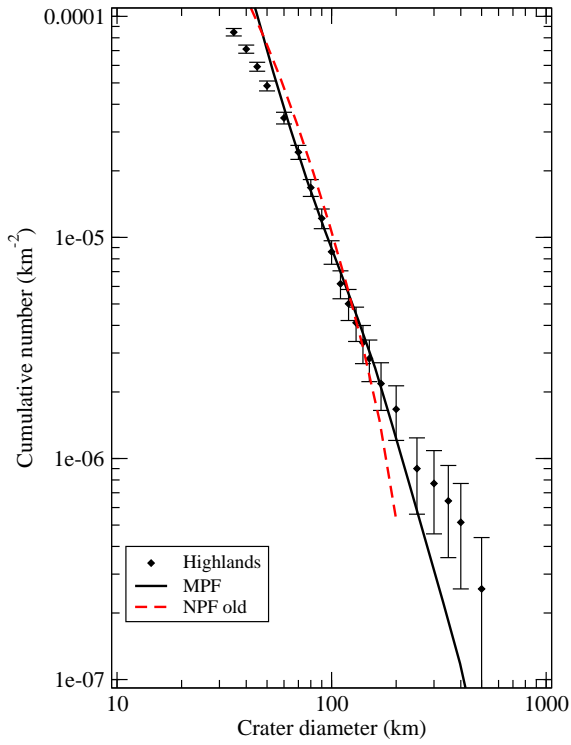


Fig. 5.— The plot shows the best fit of the crater-size cumulative distribution for the lunar highlands with both the MPF and the NPF.

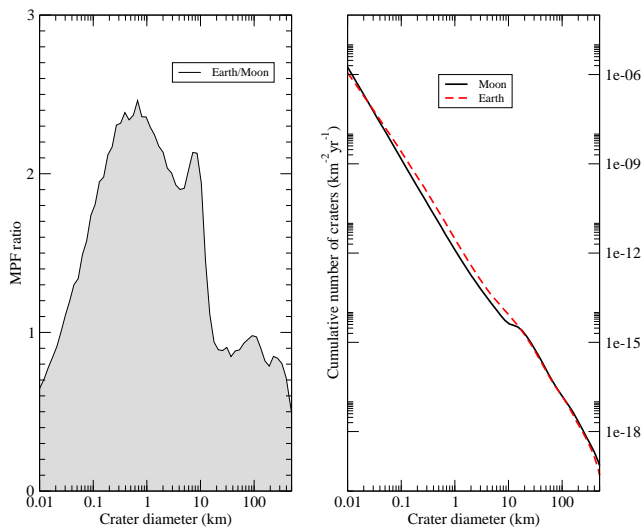


Fig. 6.— Detailed comparison of the lunar and terrestrial MPFs (using the H&H scaling law).

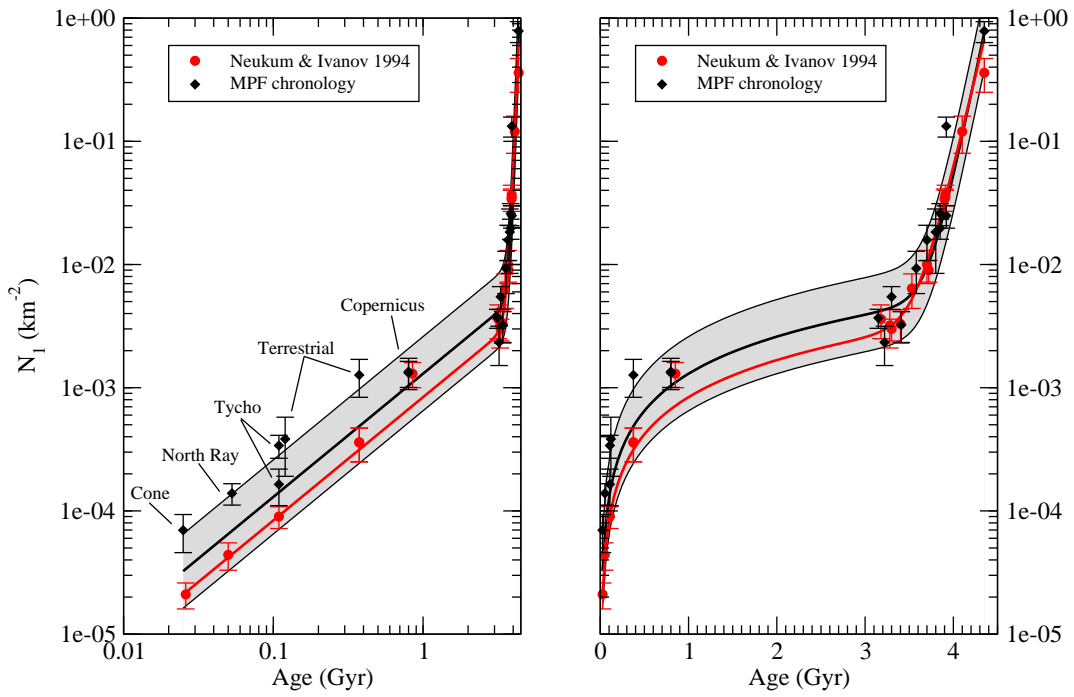


Fig. 7.— The plot shows the  $N_1$  values for the calibration regions obtained using the MPF and those obtained by Neukum & Ivanov (1994). The solid curves, namely the chronology curves, represent the best fit of the two sets of data points. The shadowed regions encompass a factor of  $\pm 2$  around the MPF chronology curve.

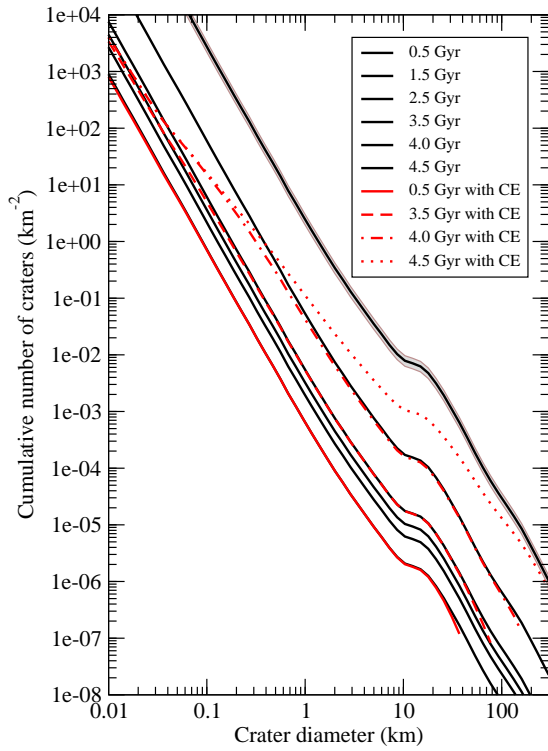


Fig. 8.— Moon isochrones obtained with  $MPF(D, 0)$ , and including the crater-erasing (CE) mechanism. The effect of longitude variations is also shown by the shadowed area for the 4.5 Gyr curve (with no erasing). The expected longitudinal asymmetry in the impactor flux has been modeled using eq. 1 of Morota et al. (2005). The impact of such analysis on the  $N_1$  values is negligible, therefore the chronology is not affected.

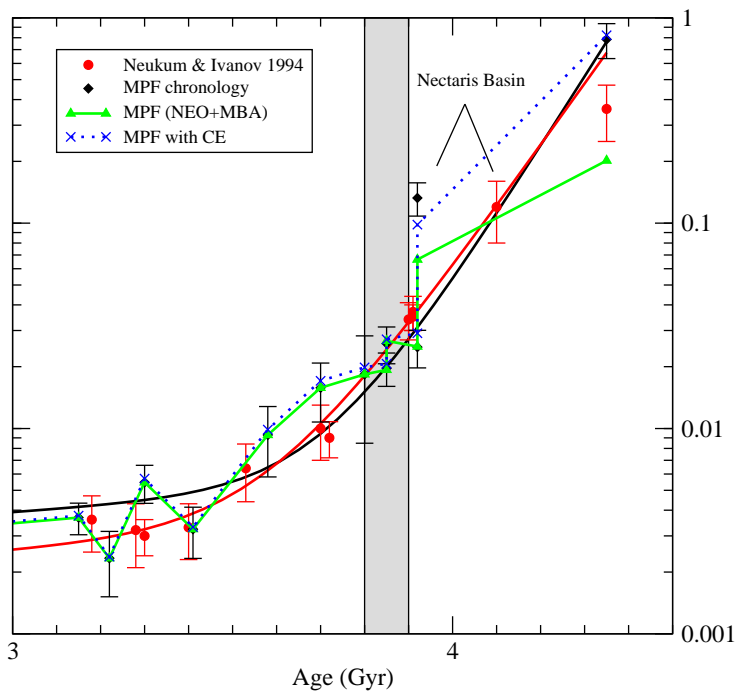


Fig. 9.— In this figure the effects of using the size distribution of MBAs and the crater-erasing (CE) mechanism are shown for the old regions alone, since the young ones are not affected. The vertical strip corresponds approximately the LHB event. Notice that for Nectaris basin the age from Stöffler & Ryder (2001) adopted in this work differs from the one in Neukum & Ivanov (1994). Moreover, the age of the highlands is known with large uncertainty and may vary in the range 4.2-4.4 Gyr. Here we adopted the values used by Neukum & Ivanov (1994).

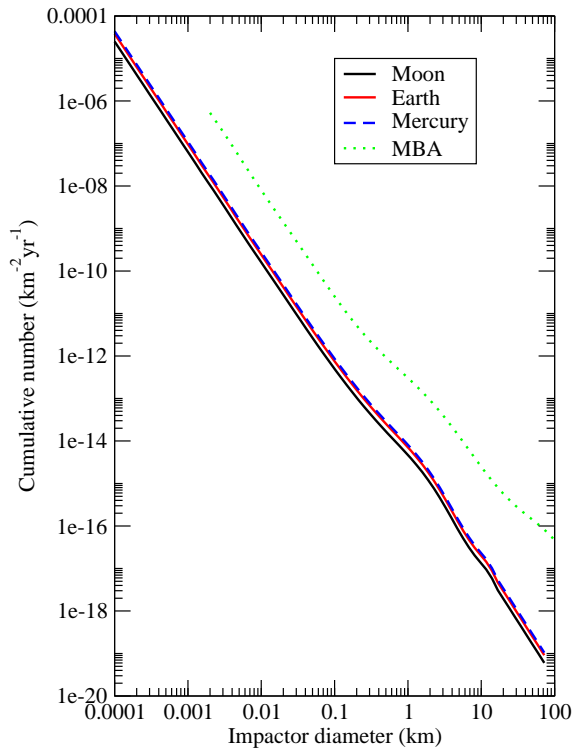


Fig. 10.— The plot shows the model cumulative distribution of impactors for Mercury, in comparison with that of the Earth-Moon system. The MBA size distribution is also shown.

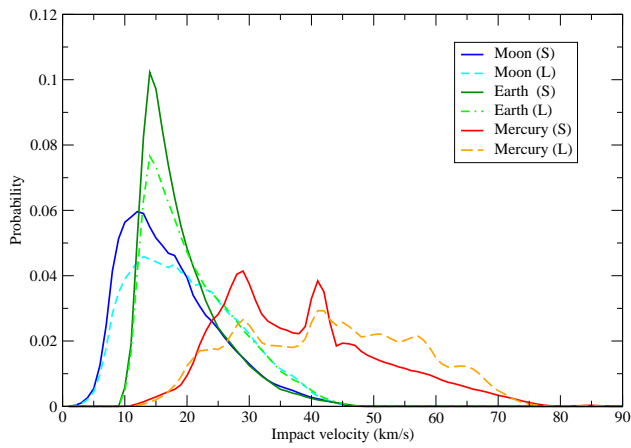


Fig. 11.— Impactor velocity distribution for Mercury, in comparison with the Earth-Moon system (see also fig. 1).



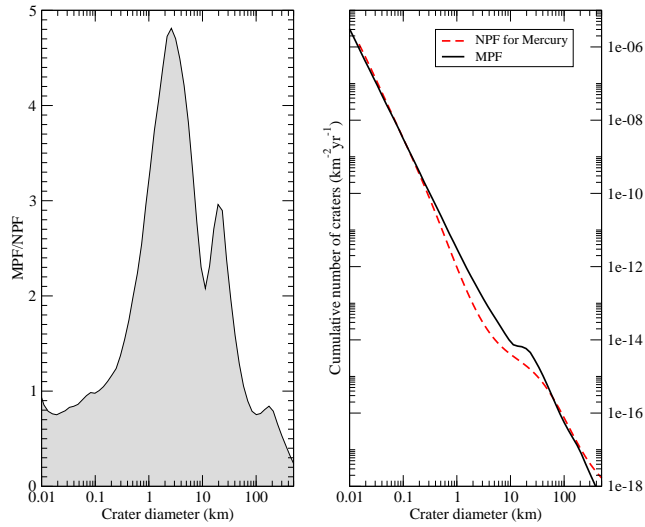


Fig. 12.— MPF for Mercury, in comparison with the NPF. The two production functions are in disagreement in the range from about 0.1 km to 40 km.

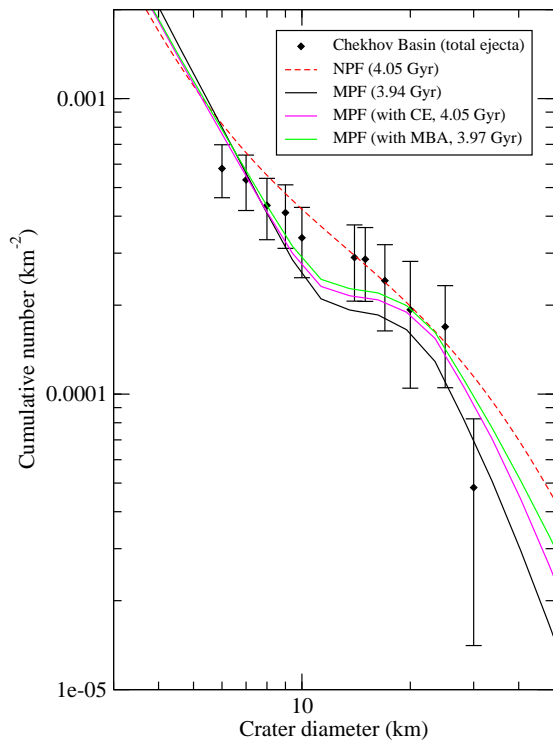


Fig. 13.— MPF best fit of Chekhov basin and derived age. We also present the best fit using the MBA size distribution and crater erasing (see section 5).

## REFERENCES

- Anderson, D. L. 2007, *New Theory of the Earth*. Cambridge University press, 380 pp.
- Asphaug, E., Moore, J. M., Morrison, D., Benz, W., Nolan, M. C., & Sullivan, R. J. 1996, *Icarus*, 120, 158
- Birck, J. L., & Allègre, C. J. 1978, *Physics of the Earth and Planetary Interiors*, 16, 10
- Bogard, D. 1995, *Meteoritics*, 30, 244
- Bottke, W. F., Vokrouhlický, D., & Nesvorný, D. 2007, *Nature*, 449, 48
- Bottke, W. F., Durda, D. D., Nesvorný, D., Jedicke, R., Morbidelli, A., Vokrouhlický, D., & Levison, H. 2005a, *Icarus*, 175, 111
- Bottke, W. F., Durda, D. D., Nesvorný, D., Jedicke, R., Morbidelli, A., Vokrouhlický, D., & Levison, H. F. 2005b, *Icarus*, 179, 63
- Bottke, W. F., Morbidelli, A., Jedicke, R., Petit, J.-M., Levison, H. F., Michel, P., & Metcalfe, T. S. 2002, *Icarus*, 156, 399
- Bottke, W. F., Jedicke, R., Morbidelli, A., Petit, J.-M., & Gladman, B. 2000, *Science*, 288, 2190
- Brown, P., Spalding, R. E., ReVelle, D. O., Tagliaferrri, E., & Worden, S. P. 2002, *Nature*, 420, 294
- Boyce, J. M., Schaber, G. G., & Dial, A. L., Jr. 1977, *Nature*, 265, 38
- Cohen, B. A., Swindle, T. D., & Kring, D. A. 2000, *Science*, 290, 1754
- Cohen, B. A., Swindle, T. D., & Kring, D. A. 2005, *Meteoritics and Planetary Science*, 40, 755
- Culler, T. S., Becker, T. A., Muller, R. A., & Renne, P. R. 2000, *Science*, 287, 1785
- Farinella, P., Vokrouhlický, D., & Hartmann, W. K. 1998, *Icarus*, 132, 378
- Fernandes, V. A., & Burgess, R. 2005, *Geochim. Cosmochim. Acta*, 69, 4919
- French, B. M. 1998. *Traces of Catastrophe: A Handbook of Shock-Metamorphic Effects in Terrestrial Meteorite Impact Structures*. LPI Contribution No. 954, Lunar and Planetary Institute, Houston. 120 pp.
- Glass, B. P. 1990, *Tectonophysics*, 171, 393
- Gomes, R., Levison, H. F., Tsiganis, K., & Morbidelli, A. 2005, *Nature*, 435, 466
- Greeley, R., & Gault, D. E. 1970, *Moon*, 2, 10
- Grieve, R. A. F., & Dence, M. R. 1979, *Icarus*, 38, 230
- Grieve, R. A. F. 1993, *Vistas in Astronomy*, 36, 203
- Halliday, I., Griffin, A. A., & Blackwell, A. T. 1996, *Meteoritics and Planetary Science*, 31, 185
- Hartmann, W.K., Strom, R., Weidenschilling, S., Blasius, K., Woronow, A., Dence, M., Grieve, R., Diaz, J., Chapman, C., Shoemaker, E., Jones K., 1981. *Chronology of planetary volcanism by comparative studies of planetary cratering*. In *Basaltic Volcanism on the Terrestrial Planets*, pp. 1050-1129. Basaltic Volcanism Study Project.
- Hartmann, W. K., Quantin, C., & Mangold, N. 2007, *Icarus*, 186, 11
- Holsapple, K. A., & Housen, K. R. 2007, *Icarus*, 191, 586
- Koeberl, C., Poag, C. W., Reimold, W. U., & Brandt, D. 1996, *Science*, 271, 1263
- Ivanov, B. A. 2001, *Space Science Reviews*, 96, 87
- Ivanov, B. A. 2006, *Icarus*, 183, 504
- Ivanov, B. A., Neukum, G., & Wagner, R. 2001, *Astrophysics and Space Science Library*, 261, 1
- Ivanov, B. A., Neukum, G., Bottke, W. F., Jr., & Hartmann, W. K. 2002, *Asteroids III*, 89
- Marchi, S., Morbidelli, A., & Cremonese, G. 2005, *A&A*, 431, 1123
- Moore, H. J., Boyce, J. M., & Hahn, D. A. 1980, *Moon and Planets*, 23, 231

- Morbidelli, A., Bottke, W. F., Jr., Froeschlé, C., & Michel, P. 2002, *Asteroids III*, 409
- Morbidelli, A., & Gladman, B. 1998, *Meteoritics and Planetary Science*, 33, 999
- Morota, T., Ukai, T., & Furumoto, M. 2005, *Icarus*, 173, 322
- Nesvorný, D., Vokrouhlický, D., Bottke, W. F., Gladman, B., Häggström, T. 2007, *Icarus*, 188, 400
- Neukum, G., & Ivanov, B. A. 1994, *Hazards Due to Comets and Asteroids*, 359
- Neukum, G., PhD Thesis, *Meteoritenbombardement und Datierung Planetarer Oberflaechen*, Munich, Feb. 1983 p 1-186
- Neukum, G., Ivanov, B. A., & Hartmann, W. K. 2001, *Space Science Reviews*, 96, 55
- Neukum, G., & Horn, P. 1976, *Moon*, 15, 205
- Neukum, G., Oberst, J., Hoffmann, H., Wagner, R., & Ivanov, B. A. 2001b, *Planet. Space Sci.*, 49, 1507
- O'Brien, D. P., Greenberg, R., & Richardson, J. E. 2006, *Icarus*, 183, 79
- Pike, R. J. 1980, *Icarus*, 43, 1
- Schmidt, R. M., & Housen, K. R. 1987, *International Journal of Impact Engineering*, 5, 543
- Shoemaker, E.M., Wolfe, R.F., Shoemaker, C.S., 1990. Asteroid and comet flux in the neighborhood of Earth. *Geological Society of America Special Paper* 247
- Stöffler, D., & Ryder, G. 2001, *Space Science Reviews*, 96, 9
- Strom, R. G., Malhotra, R., Ito, T., Yoshida, F., & Kring, D. A. 2005, *Science*, 309, 1847
- Stuart, J. S., & Binzel, R. P. 2004, *Icarus*, 170, 295
- Ryder, G. 1990, *EOS Transactions*, 71, 313
- Werner, S. C., Harris, A. W., Neukum, G., & Ivanov, B. A. 2002, *Icarus*, 156, 287
- Wilhelms, D. E. 1976, *Lunar and Planetary Science Conference*, 7, 2883

---

This 2-column preprint was prepared with the AAS L<sup>A</sup>T<sub>E</sub>X macros v5.2.